A New Stable Boundary Layer Parameterization for Weather and Forecasting Models: a Heat Flux Budget Approach

Rafael Maroneze (rafaelmaroneze@unipampa.edu.br)
Universidade Federal do Pampa
Felipe Denardin Costa
Universidade Federal do Pampa
Otávio Costa Acevedo
Universidade Federal de Santa Maria
Luiz Eduardo Medeiros
Universidade Federal do Pampa
Franciano Scremin Puhales
Universidade Federal de Santa Maria
Vagner Anabor
Universidade Federal de Santa Maria
Luca Mortarini
Institute of Atmospheric Sciences and Climate

Research Article

Keywords: Eddy diffusivity , Stable boundary layer , Turbulence parametrizations , Turbulence regime , Weather Research and Forecasting model

Posted Date: January 23rd, 2023

DOI: https://doi.org/10.21203/rs.3.rs-2442980/v1

Additional Declarations: No competing interests reported.

Version of Record: A version of this preprint was published at Boundary-Layer Meteorology on April 17th, 2023. See the published version at https://doi.org/10.1007/s10546-023-00810-4.

A New Stable Boundary Layer Parameterization for Weather and Forecasting Models: a Heat Flux Budget Approach

Rafael Maroneze · Felipe D. Costa · Otávio C. Acevedo · Luiz Eduardo Medeiros · Franciano S. Puhales · Vagner Anabor · Luca Mortarini

Received: DD Month YEAR / Accepted: DD Month YEAR

Abstract The present study introduces a new boundary layer parameterization for weather and forecasting models. It is implemented here as a boundary layer module in Weather Research and Forecasting (WRF) model. The main novelty in the new scheme is that it includes prognostic equations for the heat flux and temperature variance, being the first WRF boundary layer scheme with that feature. This is specially aimed at improving the representation of nocturnal stable boundary layer and of its turbulence regimes, weakly and very stable. The effort is supported by previous studies that found that the two regimes and the transitions between them are better represented by simplified numerical schemes that represent the interactions between the surface and the air adjacent to it when the heat flux and temperature variance are solved prognostically. The results show that the two regimes are adequately simulated by the new scheme. Such an evaluation is presented in terms of the relationship between the turbulence velocity scale and mean wind speed, of the dependence of the potential temperature gradient near the surface and the mean wind speed, and by the relationship between flux and gradient Richardson numbers. In the new scheme, the relationship between thermal structure and the mean and turbulent flows arises naturally from the heat flux prognostic equation, not being arbitrarily imposed by an empirical stability function.

Keywords Eddy diffusivity · Stable boundary layer · Turbulence parametrizations · Turbulence regime · Weather Research and Forecasting model

Rafael Maroneze
Av. Tiaraju, 810 - Ibirapuitã, Alegrete - RS, 97546-550
E-mail: rafaelmaroneze@gmail.com

1 Introduction

Through mechanical drag and thermal effects, the Earth´s surface directly affects the flow in the atmospheric boundary layer (ABL) , making it turbulent (Stull 1988; Cuxart et al. 2006). As a consequence, forecasting the mean state of the ABL demands an adequate representation of the effects of turbulence, which is usually described in turbulent models through the statistical moments of the fluctuations of the variables that describe the atmospheric flow. Furthermore, as the majority of human activities take place in the ABL, such flow is often affected by anthropogenic action. It is clear that a good representation of the ABL and its interaction with the surface is essential for all atmospheric applications.

The adequate modelling of the ABL and of its importance as a lower boundary to upper atmospheric flow has been pursued by the micrometeorological community for a long time (Taylor 1915; Blackadar 1962; Taylor and Delage 1971; Mellor and Yamada 1974; Wyngaard 1975; Louis 1979, among others). Naturally, the quality of such model representations is limited by the same difficulties that affect the bulk of knowledge of the ABL at any given historic context. Currently, a major challenge for this understanding regards the stable boundary layer (SBL), its turbulence regimes and how they relate to the mean flow and to quantities that are external to the SBL (van Hooijdonk et al. 2015; Vignon et al. 2017; van der Linden et al. 2017; Holdsworth and Monahan 2019). It has been studied by numerous authors in the last decades (Mahrt 1998; Sun et al. 2012, 2016; Acevedo et al. 2014; Mahrt 2014, among others), having been classified both observationally and in modelling in two distinct regimes: weakly stable and very stable. According to Mahrt (2014) the "*fundamental features of the very stable boundary layer still remain a mystery*". In this context, the simulation of the very SBL and the representation of transitions from and to such a regime by planetary boundary layer parameterizations is a major micrometeorological challenge that limits the quality of the representation of the mean state of the atmosphere near the surface in both numerical weather prediction (NWP) and climate models today {(van de Wiel et al. 2017; Battisti et al. 2017; Baas et al. 2019; Holdsworth and Monahan 2019; Lapo et al. 2019; Maroneze et al. 2019, 2021; Lorenz et al. 2022; Kähnert et al. 2022). At the same time, the weakly SBL is well described by Monin-Obukhov similarity theory and, for this reason, is comparatively well simulated and represented by numerical planetary boundary layer (PBL) parametrization schemes (Mahrt 2014).

The Weather Research and Forecasting (WRF) model (Skamarock et al. 2008) is largely employed to investigate hydrology, renewable energy, regional climate, weather prediction, and other phenomena (Powers et al. 2017), both for scientific research and for operational numerical prediction. Maroneze et al. (2021) have analyzed the quality of the representation of turbulence in very stable conditions by the different WRF PBL parameterizations that solve the turbulence kinetic energy, either diagnostically or prognostically. They found that the variety of existing parameterizations lead to a large diversity in representations between turbulent and mean quantities, with different simulated thresholds between the two regimes and consequent very different predictions of mean quantities in specific situations. None of the boundary-layer parameterizations available in WRF solves a prognostic equation for the heat flux, although there are indications in the literature that this variable has a decisive control in the the SBL turbulence regime (van de Wiel et al. 2012; Maroneze et al. 2019). Maroneze et al. (2019) have shown that the adequate simulation of the transition between the two regimes is much better simulated when a prognostic for the heat flux is solved by a prognostic equation, rather than represented by a parmeterization.

In NWP models, the influence of flow stability to the ABL flow is usually prescribed as an empirical and arbitrary stability function (Costa et al. 2020). Here, it is hypothesized that the model flow dependence on stratification, and, more generally, the relationship between mean and turbulence quantities (such as the flux and gradient Richardson numbers) arises naturally in the model when the heat flux is prognostically solved, instead of being prescribed by a stability function. Therefore, the main goal of the present study is to introduce a new stable boundary layer parameterization for weather and forecasting models that includes prognostic equations for the heat flux and temperature variance. Such a scheme is implemented in the WRF model version 3.9, described in section 2. The proposed parametrization is calibrated and validated using GEWEX Atmospheric Boundary Layer Study (GABLS) I (Kosović and Curry 2000) as a control case, in section 3.2. The ability of the new parameterization to represent the two contrasting SBL regimes is evaluated in section 4, through the relationships it simulates between the turbulence velocity scale and the mean wind speed, between the potential temperature gradient near the ground surface and the mean wind speed, and between the flux and gradient Richardson numbers.

2 Description of the Planetary-Boundary-Layer Parametrization

Turbulence affects the mean state of the planetary boundary layer through the divergence of turbulent fluxes. Such a divergence in the vertical direction is often the dominant process affecting mean quantities near the surface. When its role is sufficiently larger than that of other influences, the prognostic equations for mean horizontal velocity components and potential temperature may be regarded as

$$\left[\frac{\partial \overline{u}}{\partial t}\right]_{PBL} = -\frac{\partial \overline{u'w'}}{\partial z}, \tag{1}$$

$$\left[\frac{\partial \overline{v}}{\partial t}\right]_{PBL} = -\frac{\partial \overline{v'w'}}{\partial z}, \tag{2}$$

$$\left[\frac{\partial \overline{\theta}}{\partial t}\right]_{PBL} = -\frac{\partial \overline{w'\theta'}}{\partial z}. \tag{3}$$

In equations (1-3) $\overline{u}$, $\overline{v}$ and $\overline{\theta}$ are respectively the mean velocity components in zonal and meridional directions, and the mean potential temperature. The vertical turbulent momentum fluxes are given by $\overline{u'w'}$ and $\overline{v'w'}$, while $\overline{w'\theta'}$ is the turbulent heat flux.

According to K theory, the vertical turbulent momentum fluxes are parametrized as (Mellor and Yamada 1974, 1982; Therry and Lacarrere 1983; Bougeault and Lacarrere 1989; Janjić 1994; Nakanishi and Niino 2009; Bretherton and Park 2009, among others)

$$\overline{u'w'} = -K_m \frac{\partial \overline{u}}{\partial z}, \tag{4}$$

and

$$\overline{v'w'} = -K_m \frac{\partial \overline{v}}{\partial z}, \tag{5}$$

where K_m is the vertical turbulent diffusion coefficients for momentum. In turbulence closures that solve the TKE either prognostically or diagnostically, it is common to estimate K_m as a function of TKE, the mixing length l_m, and a stability function f_m (Mellor and Yamada 1974, 1982; Nakanishi and Niino 2009; Bretherton and Park 2009; Costa et al. 2020, among others)

$$K_m = \sqrt{\overline{e}}\; l_m f_m. \tag{6}$$

For a horizontally homogeneous atmosphere, the prognostic equation for TKE ($\overline{e}$) is

$$\frac{\partial \overline{e}}{\partial t} = -\overline{u'w'}\frac{\partial \overline{u}}{\partial z} - \overline{v'w'}\frac{\partial \overline{v}}{\partial z} + \frac{g}{\Theta}\overline{w'\theta'} - \frac{\partial}{\partial z}\left[\overline{w'e} + \frac{\overline{p'w'}}{\rho_0}\right] - \epsilon_e, \tag{7}$$

where p is pressure, ρ_0 is a reference density and Θ is a reference temperature. In the right hand side (r.h.s) of Eq. 7, the first and second terms represent the turbulence shear production (SP);the third term is the turbulence buoyant destruction (production) under stable (unstable) conditions (BD/P); the fourth term is the vertical transport of TKE both by turbulence and by pressure fluctuations (TR); and the fifth term is TKE viscous dissipation (DIS).

The TKE viscous dissipation (ϵ_e) can be paramererized as a function of TKE and a characteristic dissipation length l_ϵ:

$$\epsilon_e = c_1 \frac{\overline{e}^{3/2}}{l_\epsilon}, \tag{8}$$

where c_1 is a numerical constant. According to Cuxart et al. (2006), values from 0.08 to 0.7 have been used for c_1.

Following Duynkerke (1988), the TKE transport term is represented as:

$$-\frac{\partial}{\partial z}\left[\overline{w'e} + \frac{\overline{p'w'}}{\rho_0}\right] = \frac{\partial}{\partial z}\left[K_e \frac{\partial \overline{e}}{\partial z}\right], \tag{9}$$

here $K_e = \alpha_e K_M$.

The prognostic equation for the heat flux ($\overline{w'\theta'}$) is:

$$\frac{\partial\overline{w'\theta'}}{\partial t} = -\overline{w'^2}\frac{\partial\overline{\theta}}{\partial z} + \frac{g}{\Theta}\overline{\theta'^2} - \frac{\partial\overline{w'w'\theta'}}{\partial z} + \frac{1}{\rho_0}\overline{\theta'\frac{\partial p'}{\partial z}}, \tag{10}$$

where the first term on the r.h.s represents the thermal gradient production of heat flux in a SBL (TGP). The second term is heat flux buoyant destruction (production) under stable (unstable) condition, and the third term represents the transport of heat flux by turbulence, while the fourth term either one or the other both the transport by pressure fluctuations and return-to-isotropy.

Following Therry and Lacarrere (1983) the last term of Eq. 10 is parameterized according to the idea of a pressure relaxation, as the sum of two contributions. The first is proportional to the heat flux ($P1$) itself and the second is proportional to the temperature variance ($P2$)

$$\frac{1}{\rho_0}\overline{\theta'\frac{\partial p'}{\partial z}} = P1 + P2, \tag{11}$$

where

$$P1 = -c_2\frac{\overline{e}^{1/2}}{l_\epsilon}\overline{w'\theta'} \quad \text{and} \quad P2 = -c_3\frac{g}{\Theta}\overline{\theta'^2}, \tag{12}$$

and c_2 and c_3 are numerical constants.

For temperature variance, the prognostic equation is:

$$\frac{\overline{\partial\theta'^2}}{\partial t} = -2\overline{w'\theta'}\frac{\partial\overline{\theta}}{\partial z} - \frac{\partial\overline{w'\theta'^2}}{\partial z} - \epsilon_\theta, \tag{13}$$

where the first term in the r.h.s is the heat flux production of temperature variance (Pr), the second is its turbulent transport (TR) and the third term is its molecular dissipation (DIS).

The dissipation term of temperature variance is parametrized as

$$\epsilon_\theta = c_4\frac{\sqrt{\overline{e}}}{l_\epsilon}\overline{\theta'^2}, \tag{14}$$

where c_4 is numerical constants.

In analogy with Eq. 9, the transport term in Eqs. 10 and 13 are parametrized as

$$-\frac{\partial\overline{w'w'\theta'}}{\partial z} = \frac{\partial}{\partial z}\left[K_e\frac{\partial\overline{w'\theta'}}{\partial z}\right] \text{and } -\frac{\partial\overline{w'\theta'^2}}{\partial z} = \frac{\partial}{\partial z}\left[K_e\frac{\partial\overline{\theta'^2}}{\partial z}\right].$$

To close the above set of equations, the numerical constants, the mixing length l_m and the characteristic dissipation length l_ϵ must be specified. In the literature, the two mixing lengths are generally taken as equal to each other (Therry and Lacarrere 1983; Weng and Taylor 2003; Costa et al. 2020, among other) and many different formulations and numerical constants have already been proposed.

WRF uses an Arakawa C grid, where the center of the grid cell (represented by symbol × in fig. 1) are referred as "mass points" or full levels, while the face grid points staggered at one-half grid length from the mass points are referred as half levels (represented by symbol ◯ in fig. 1). Here, the prognostic equations for any turbulent variables are calculated at the full levels, in contrast with other parameterizations present in WRF. Therefore, here the turbulent flux divergences can be estimated directly through centered finite differences, not being necessary the use of spatially averaged values (Fig. 1).

Equations (7),(10), and (13) are solved through an implicit time-integration method. They can be generically discretized as

$$\underbrace{\frac{\Psi_k^{n+1} - \Psi_k^n}{\Delta t}}_{\text{tendency}} = \underbrace{\frac{\partial}{\partial z}\left[K_m^n \frac{\partial}{\partial z}\Psi^{n+1}\right]_k}_{\text{Transport}} + \underbrace{P_k^n}_{\substack{\text{Production}\\\text{Destruction}}} - \underbrace{F_k^n \Psi_k^{n+1}}_{\text{Dissipation}}, \tag{15}$$

where Ψ is the turbulent variable, n denotes the time index and k denotes the vertical full level index. Equation (15) is integrated in time by the relationship

$$a\,\Psi_{k-1}^{n+1} + b\,\Psi_k^{n+1} + c\,\Psi_{k+1}^{n+1} = d \tag{16}$$

where a, b, and c are the elements of the matrix that solves the implicit system for Ψ_{k-1}^{n+1}.

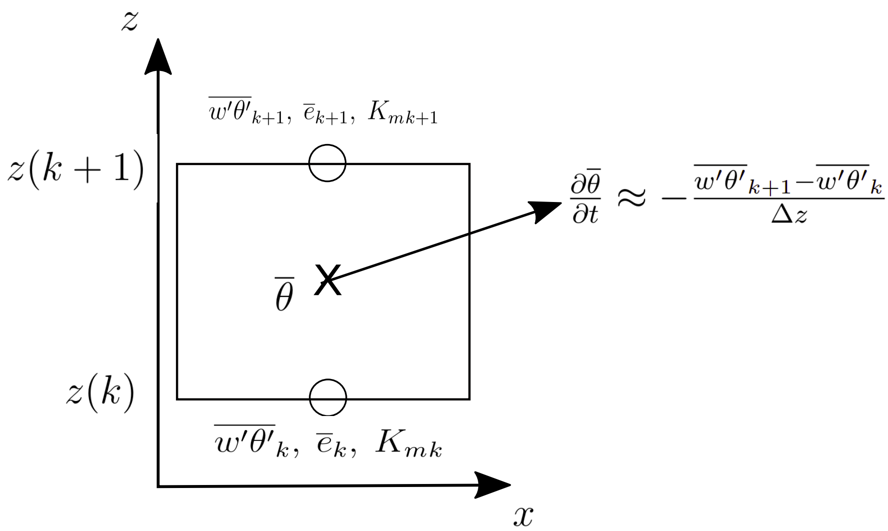

Fig. 1 The schematic representation of vertical adapted Arakawa C grid for the present PBL parametrization.

3 Model Validation

3.1 Control Case and model discretization

PBL schemes are typically calibrated through a control case. One of the most widely used reference cases for such a purpose is the first Global Energy and Water cycle EXperiment (GEWEX) Atmospheric Boundary Layer Study (GABLS I). GABLS I provides a model intercomparison for SCM (Cuxart et al. 2006) and LES (Beare et al. 2006) for a weakly stable boundary layer, with prescribed temperature at the surface (Kosović and Curry 2000). Over the years, GABLS I has been used to validate schemes designed for different purposes, such as the development of new parametrizations (Bretherton and Park 2009; Cheng et al. 2020), SBL regimes regime transitions studies (Costa et al. 2020).

The boundary and initial conditions used in all simulations described in this section are the same as those in GABLS I (Kosović and Curry 2000; Cuxart et al. 2006):

- Constant geostrophic wind components ($u_G = 8$ m s^{-1} and $v_G = 0$ m s^{-1}) at the domain top, along the entire simulation;
- Constant surface cooling rate (0.25 K h^{-1}) along the simulation;
- The initial profiles of wind components, temperature and turbulence kinetic energy are: $\overline{u}(z,t=0) = u_G$; $\overline{v}(z,t=0) = v_G$; $\overline{\theta}(z < 100 \text{ m}, t=0) = 263.5$ K, while a constant lapse rate of 0.1 K m^{-1} is considered at heights $z > 100$ m; $\overline{e} = 0.4(1 - z/250)^3$.

WRF single column mode (WRF-SCM), with 170 levels between the surface ($z = 0$) and the domain top ($z = 6$ km), is used in the PBL scheme validation. The first atmospheric level is fixed at $z = 1.5$ m, and the grid spacing increases steadily from 1.6 m near the surface, to 198 m near the domain top.

3.2 Model calibration

Typically, PBL schemes implemented in weather and climate models have a large number of tuning parameters. The number of numerical constants is proportional to the number of parametrizations necessary to close the system of equations. According to Audouin et al. (2021), the model calibration consists in adjusting each tuning parameter, by taking into account both the model performance and physical restrictions. It can be a difficult task because of the large number of degrees of freedom which demand a high computational cost (Audouin et al. 2021).

3.2.1 Stable Boundary Layer Mixing Length Formulation

An adequate mixing length formulation is crucial to properly describe the boundary layer flow (Weng and Taylor 2003), having a very important role in any PBL scheme. In the literature, many different formulations have been proposed. Blackadar (1962) suggested

$$\frac{1}{l_{Blackadar}} = \frac{1}{\kappa z} + \frac{1}{\lambda_0}, \tag{17}$$

where $l_{Blackadar}$ is a mixing length, κ is von Karman constant, and λ_0 is a reference length scale. Table 1 show different formulations for λ_0 proposed in the literature.

The mixing length tends to be smaller under stable thermal stratification (André et al. 1978), and can be given by the harmonic average between $l_{Blackadar}$ and a buoyant length scale L_B (Sukoriansky et al. 2005; Nakanishi and Niino 2009, among other)

$$\frac{1}{l_m} = \frac{1}{l_{Blackadar}} + \frac{1}{L_B}, \tag{18}$$

where

$$L_B = C_N \frac{\sqrt{2\ \overline{e}}}{N}, \tag{19}$$

where N is the Brunt–Väisälä frequency and C_N is a numerical constant whose used values range from 0.2 to 1 (André et al. 1978; Baas et al. 2008; Nakanishi and Niino 2009).

The role of the reference length scale can be evaluated by considering $L_B \to \infty$ in Eq. (18) and varying λ_0. Fig. 2 shows that the mean vertical profiles of the different atmospheric quantities vary largely with λ_0. For example, the height and width of the near surface maxima of the wind-velocity profile increases linearly with λ_0 (Fig. 2a,b). The absolute values of momentum flux $\left(\tau/\rho = \sqrt{\overline{u'w'}^2 + \overline{v'w'}^2}\right)$, potential temperature ($\overline{\theta}$), heat flux ($\overline{w'\theta'}$), temperature variance ($\overline{\theta'^2}$), vertical wind velocity variance component ($\overline{w'^2}$), and TKE ($\overline{e}$) and the momentum eddy viscosity (K_m) generally increase at all heights as λ_0 increases. When compared to the GABLS1 observations, the simulated TKE is underestimated for most of the values of λ_0 considered. In general, the comparison indicates that when $\lambda_0 = 2$ m, the model outputs are closest to the GABLS1 reference case (Fig. 2 c-i). However, the intensity of the wind-speed maximum near the surface (low-level-jet nose, Klein et al. 2016) is underestimated. For larger values of λ_0, the temperature variance increases with height until it reaches a maximum near the SBL top (Fig. 2f). When λ_0 is evaluated by formulations such as those proposed by Mellor and Yamada (1974) (MY, black dashed lines in Fig. 2) and Bretherton and Park (2009) (UWBLS, yellow lines in Fig. 2) the mean vertical profiles of the atmospheric quantities approach their values when large values of λ_0 are considered.

Finite values of the buoyant length scale, in Eq. (18), make the wind-speed maximum near the surface sharper and more intense. Moreover, it reduces the turbulence intensity promoting a shallower SBL (not shown). The value chosen for C_N is important because the buoyant length scale plays a similar

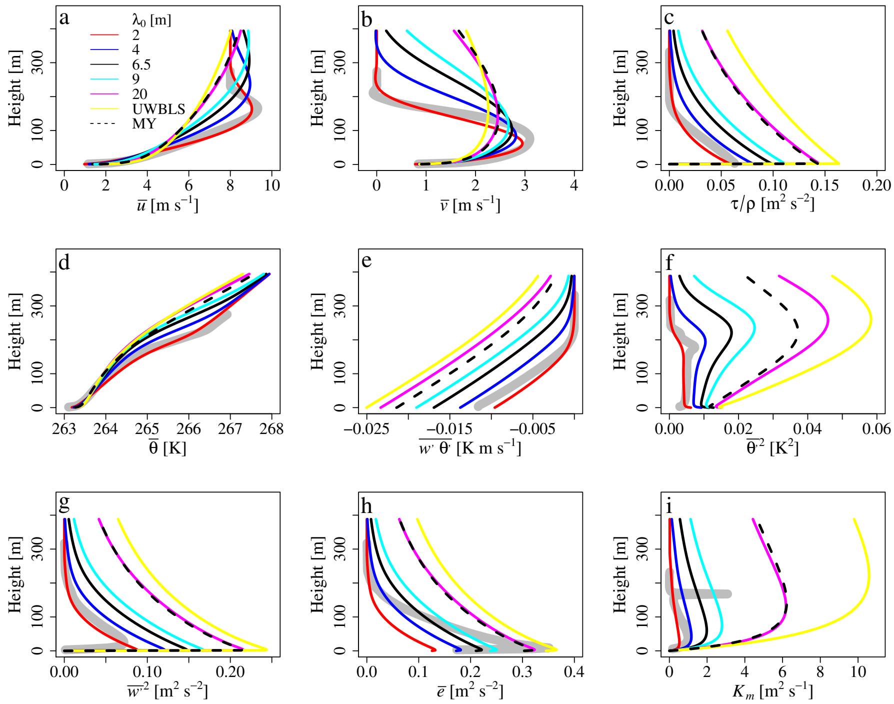

Fig. 2 Vertical profiles, mean values taken over last two hours from the simulation of zonal and meridional velocity components $\overline{u}$ (a) and $\overline{v}$ (b), the absolute values of momentum flux τ/ρ (c), potential temperature $\overline{\theta}$ (d), kinematic heat flux $\overline{w'\theta'}$ (e), temperature variance $\overline{\theta'^2}$ (f), vertical wind velocity variance component $\overline{w'2}$ (g), TKE (h), and the momentum eddy viscosity K_m (i) for different reference length scales. The solid thick gray line is the GABLS I case.

role as a stability function does in the mixing length formulation under stable conditions (Fig. 3). When smaller values of C_N are considered, the profiles of the wind speed components present a sharper and more intense maximum than when C_N is larger (Figs. 3a,b). On the other hand, in those cases the momentum eddy diffusivity is smaller than in the cases with large C_N (Fig. 3i). This occurs because the buoyant length scale will decrease, for small C_N, and then, it will reduce the mixing length intensity and the diffusion coefficients, consequently. When large values of C_N are assumed the momentum flux, the heat flux, the temperature variance and TKE become more intense (Fig. 3c,e,f,h), determining a more turbulent and deeper SBL. Even though the turbulence intensity increases with C_N, the temperature vertical profile shows that the SBL will become colder near the the boundary layer top because the enhanced turbulent transport allows the cold air reaching higher levels (Fig. 3d). In almost all comparisons between the profiles presented in Fig. 3, one can verify that the model profiles are closer to the control case when the parameters λ_0 = 6.5 m and C_N= 0.2 are used. Therefore, in order to keep the parametrization as simple and as accurate as possible, such optimized values of λ_0 and C_N are used in the following analysis.

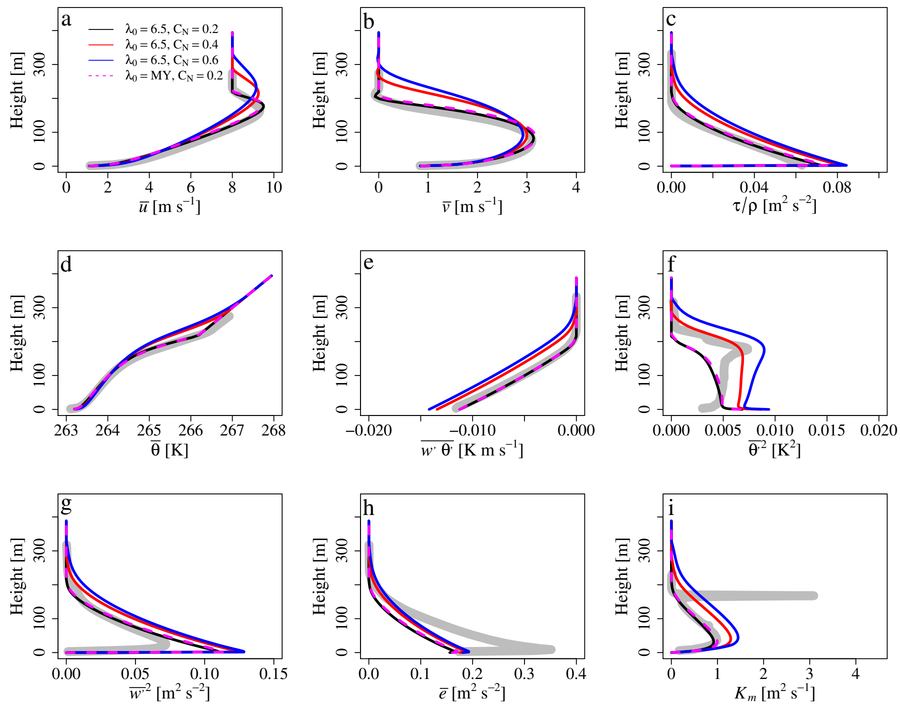

Fig. 3 Same of Fig. 2 considering a finite values of the buoyant length scale and different values of C_N.

Table 1 Reference length scale

Reference	λ_0 [m]
Blackadar (1979)	$0.00027\frac{U_G}{f}$
Bretherton and Park (2009)	$0.085\ PBLH$
Mellor and Yamada (1974)	$0.1\frac{\int_0^\infty \|z\|qdz}{\int_0^\infty qdz}$
Therry and Lacarrere (1983)	50
QNSE	$0.0063\frac{u_*}{f}$

3.2.2 Second order constants dependence

As mentioned in section 2, the value of c_1 in the parameterization of tke viscous dissipation (Eq. 8), varies by almost an order of magnitude among existing

PBL schemes. Fig. 4 shows how the variation of c_1 impacts the model. All profiles show that the SBL height decreases appreciably as c_1 increases (Fig. 4). When larger values of c_1 are considered, the magnitudes of momentum flux, heat flux, temperature variance, TKE, and momentum eddy diffusivity become smaller and a shallower SBL is simulated (Fig. 4c,e,f,h,i). Increasing c_1 leads to larger TKE dissipation, reducing the turbulent quantities and causing the SBL to be more stratified. Moreover, the turbulent flux divergence also varies, affecting the vertical potential temperature profile, which is nearly linear in the SBL (Fig. 4d) for large c_1 values, while it is curved, which a smaller stratification at lower levels when c_1 is smaller.

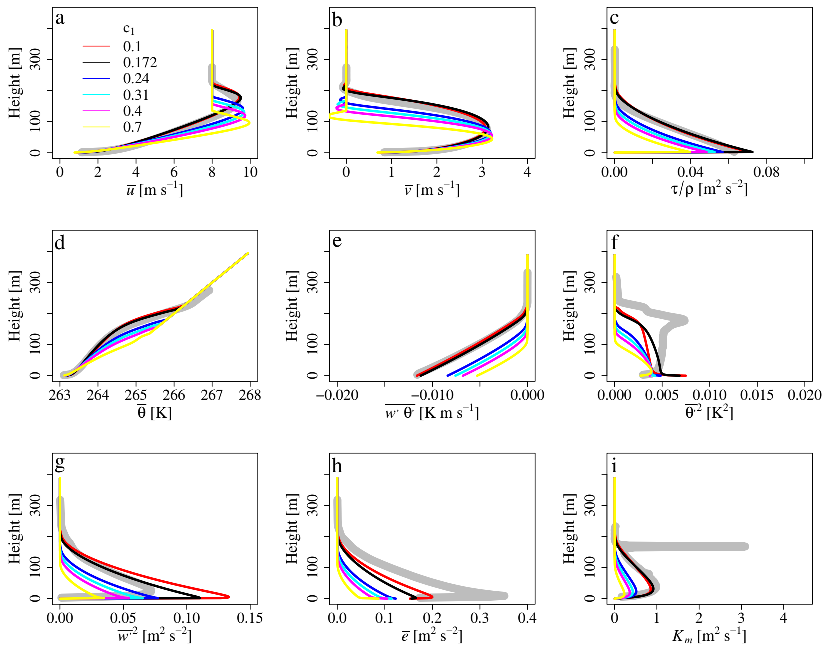

Fig. 4 Same of Fig. 2 for different values of c_1 in the parametrization of tke viscous dissipation.

While c_1 values impact the SBL depth, the choice of parameters c_2 and c_3 (Eq. 12) does not have the same effect. On the other hand, varying c_2 affects the vertical profiles of temperature (Fig. 5a), heat flux (Fig. 5b) and of the mean temperature variance (Fig. 5c). The constants c_2 and c_3 are, respectively, control parameters in the parameterization of the transport by pressure fluctuations and in the return-to-isotropy terms in the heat flux budget (Eq. 10). In particular, c_2 is a coefficient in the parameterization that mimics a heat flux dissipation rate (P_1). Therefore, larger values of c_2 cause a decrease on the simulated heat flux magnitude (Fig. 5b), consequently reducing variance as well (Fig. 5c). Furthermore, smaller values of c_2 imply larger absolute heat, allowing larger turbulent heat transport at levels near the SBL top, which becomes colder (read line in Fig. 5a), although not affecting the SBL thickness. In such case, the stability of the entire SBL is reduced, and it becomes a near-neutral layer from the ground until near the top, where a large thermal inversion is present. As the temperature variance production is proportional to both the heat flux and the thermal gradient, in this case the temperature variance is small for most of the SBL, reaching a local maximum near the maximum of the thermal gradient, at the SBL top (red line in Fig. 5c). Fig. 5 also shows that the SBL height is not affected by the choice of free coefficient in the temperature variance dissipation rate (c_4). A 4-fold variation in c_4 causes the surface heat flux to vary by less than 11 % (Fig. 5e).

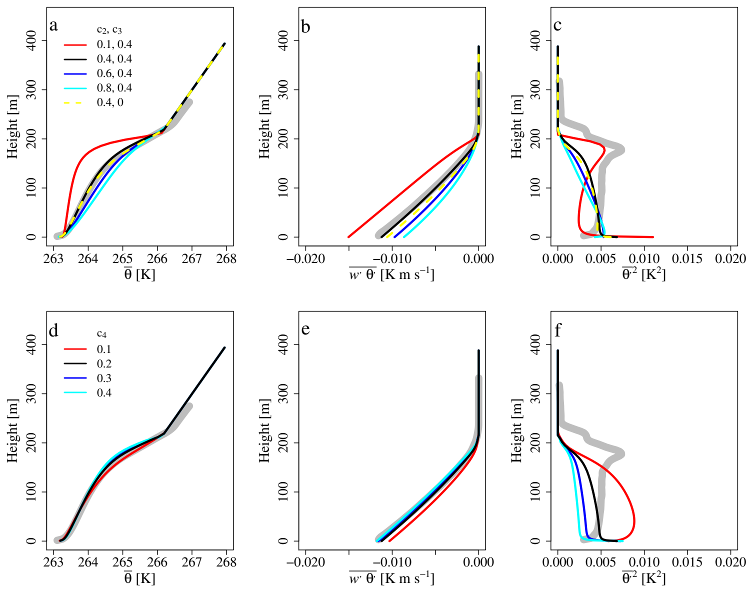

Fig. 5 Vertical profiles, mean values taken over last two hours from the simulation, for potential temperature $\overline{\theta}$ (a, d), kinematic heat flux $\overline{w'\theta'}$ (b, e), temperature variance $\overline{\theta'^2}$ (c, f) for different values of c_2, c_3 and c_4. The solid thick gray line is the GABLS I case.

Based on these results, the free parameters of the model have been chosen to optimize the model performance, when the outputs are compared with the values from GABLS I case (Table 2). Such a comparison is shown in Fig. 6 for PBL height (Fig. 6a), surface sensible heat flux (Fig. 6b) and the surface friction velocity (Fig. 6c). Following Cuxart et al. (2006), in this analysis the boundary-layer height is the level where the sensible heat flux decays to 5% of its surface value.

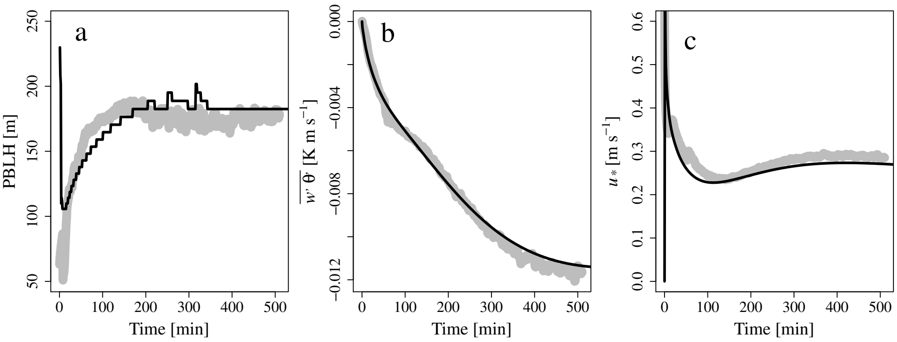

Fig. 6 PBL height (a), heat flux (b), and friction velocity (c) temporal evolution. The solid thick gray points is the GABLS I case.

Table 2 Free Parameter

c_1	0.172
c_2	0.4
c_3	0.4
c_4	0.2
c_N	0.2
α_e	3

4 SBL Regimes

The methodology employed to evaluate whether the newly proposed PBL scheme correctly reproduces the physical properties of both SBL turbulence regimes is similar to that employed by Maroneze et al. (2021). The geostrophic zonal velocity component u_G is assumed to be temporally and vertically constant for each simulation. Values of u_G considered varied from 0.5 m s^{-1} to 24 m s^{-1}, with 0.5 m s^{-1} steps between 0.5 and 14 m s^{-1}, and with 1 m s^{-1} steps between 14 and 24 m s^{-1}. In this section the skin temperature is estimated through the Unified Noah Land Surface Model (Mukul Tewari et al. 2004), while the RRTM Longwave Scheme (Mlawer et al. 1997) and the Dudhia Shortwave Scheme (Dudhia 1989) are adopted for radiative processes. The Purdue Lin scheme (Chen and Sun 2002) has been used to represent the microphysical process. For all simulations one dryland cropland and pasture land vegetation with vegetation fraction of 0.5 are considered. The roughness length for this surface type is 0.15 m.

The SBL turbulence regime transition can be determined from both local and bulk variables. Initially, both SBL regime classifications and regime transitions have been marked in terms of stability parameters (Mahrt 1998). However, the use of a single stability parameter such as the Obukhov length, or the Richardson number (either in its flux or gradient form), is ineffective at distinguishing the SBL regimes universally (Monahan et al. 2015). On the other hand, since the mean wind speed has a crucial control on the SBL regime, it has become common practice to assess it through the relationship among turbulent quantities, such as the turbulence velocity scale ($V_{TKE} = \sqrt{\overline{e}}$), and the mean wind speed (Sun et al. 2012; van de Wiel et al. 2012; Acevedo et al. 2016, 2019, among others).

The study of Sun et al. (2012) established the relationship between V_{TKE} and $\overline{U}$ as a criterion to determine the local SBL regime (Acevedo et al. 2016, incluir varios). In general, V_{TKE} increases linearly with $\overline{U}$ in both regimes, but the rate of increase is notably larger in the weakly stable than in the very stable regime. Therefore, the regime transition occurs at the value of $\overline{U}$ for which the slope of such a relationship changes abruptly (Sun et al. 2012). The scheme presently proposed simulates a very stable regime, characterized by a subtle V_{TKE} increase as $\overline{U}$ increases, in general agreement with the observations. It is important to notice that for very weak winds speeds, V_{TKE} sometimes assumes a constant value that is equal to minimum value imposed to the scheme. Contrastingly, when the wind speed is larger, a weakly stable regime is simulated, with V_{TKE} increasing rapid as $\overline{U}$ increases (Fig. 7). The change between the two slopes is abrupt, craracterizing the value of $\overline{U}$ for which the SBL regime transition occurs (Fig. 7). Maroneze et al. (2021) compared the relationship between V_{TKE} and $\overline{U}$ for six different boundary layer schemes that explicitly or implicitly solve TKE in WRF: Mellor-Yamada Nakanishi Niino 2.5 (MYNN2.5), Mellor-Yamada Nakanishi Niino 3.0 (MYNN3.0), Mellor Yamada-Janjic (MYJ) Quasi-Normal Scale Elimination (QNSE), University of Washington (UWBLS) and Bougeault-Lacarrére (BouLac). Among these, only MYNN2.5 was able to reproduce both SBL regimes and the transition between them as according to the observations as does the scheme presently proposed. The others typically simulate poorly the very-stable regime, as V_{TKE} varies little of nothing as $\overline{U}$ increases.

The SBL regime transition is also clear when the temperature difference near the ground is considered (Fig. 8). As shown by Vignon et al. (2017), the near surface potential temperature difference reaches its larger values for weak wind speeds, when turbulence is not strong enough to mix the whole layer, so that the lower levels become decoupled from higher levels. As the mean wind speed increases, the potential temperature difference starts to decreases sharply characterizing the regime transition (Fig. 8). Moreover, for large wind speeds the temperature difference tends to very small values, because the turbulence is sufficient to keep the bottom and top of the layer coupled. Maroneze et al. (2021) have shown that the relationship between the vertical temperature difference and the mean wind speed is not well solved by the many turbulence schemes used in WRF. Besides, the solutions of the different schemes are largely variable in terms of the thermal gradient they simulate in the limits of small and large wind speed, or in terms of how abrupt is the variation of such a gradient with wind speed at the regime transition. In the present scheme, a temperature difference of 3.5 K between 1 and 30 m is simulated under low

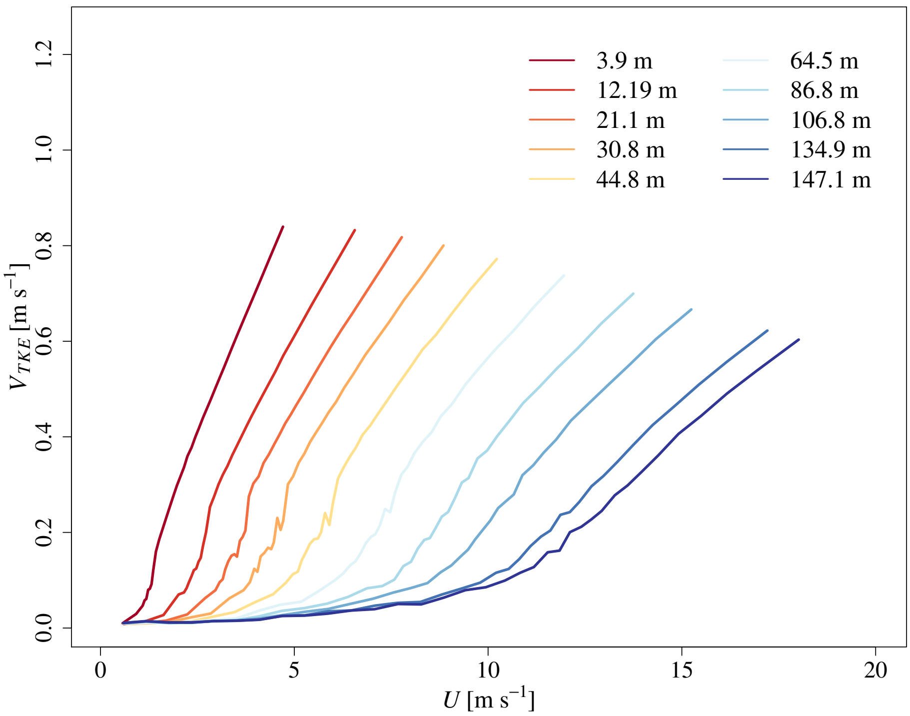

Fig. 7 Average turbulence velocity scale V_{TKE} as a function of the mean wind speed U.The panel shows bin-averaged values taken from the all night of simulation, considering all runs.

winds, dropping below 1 K as the 30-m wind speed exceeds 5 m s^{-1}. In general, the new formulation leads to smaller thermal gradients than MYNN2.5, and a more abrupt transition. In Fig. 8, these results are compared to those obtained with MYNN2.5, that was found to best reproduce the regime transition among those schemes compared by Maroneze et al. (2021). Particularly, the reduced thermal gradients in the weakly stable regime are confirmed by CASES-99 observations (Sun et al. 2012; Acevedo et al. 2021). The difference is partially a consequence that the present scheme lacks a stability function, so that the dependence on stratification arises naturally from the heat flux prognostic equation.

The turbulent Prandtl number is defined as the ratio between the momentum eddy diffusivity and the heat diffusivity ($Pr_T = K_M/K_H$). Generally, PBL schemes use a constant value for Pr_T, thus estimating the turbulent heat diffusivity (K_H). Such a use of a constant Pr_T implies that the ratio between the flux (Ri_f) and gradient (Ri_g) Richardson numbers is also constant, since $Pr_T = Ri_g/Ri_f$. However, both atmospheric data and laboratory experiments show that only in the weakly stable regime Ri_f increases linearly with Ri_g, implying a constant Pr_T (Zilitinkevich et al. 2013), whose value may be from 0.7 to 0.9 (Basu and Holtslag 2021). On the other hand,

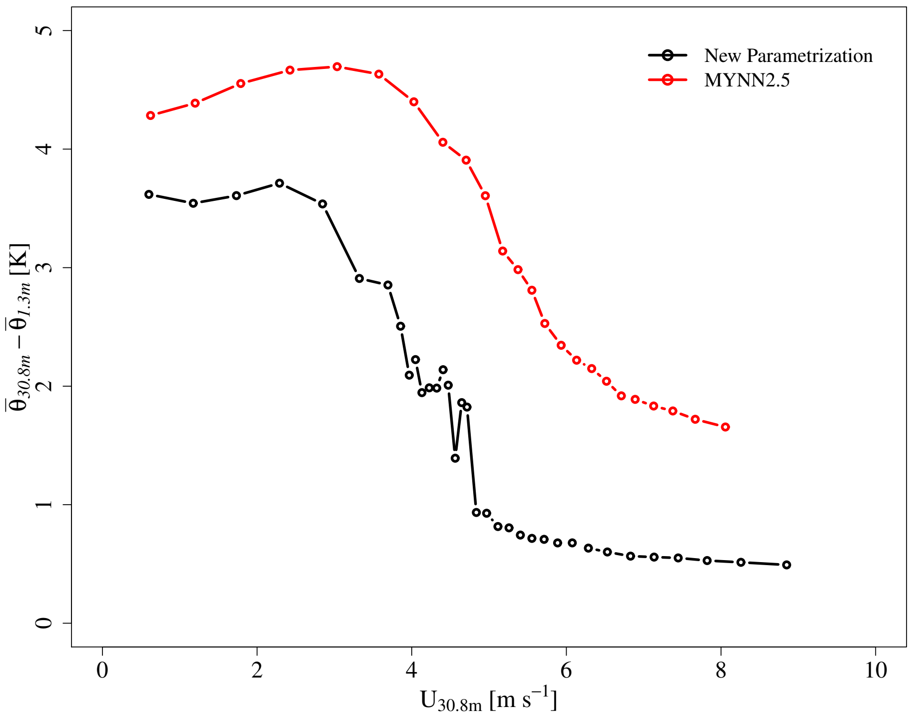

Fig. 8 Average potential temperature difference between 30.8 and 1.3 m as a function of the 30.8-m wind speed for each PBL parametrization, according to the legend. The panel shows bin-averaged values taken from the all night of simulation, considering all runs.

observations show that when Ri_g exceeds a critical value ($Ri_g \approx 0.2$), Ri_f tends to a finite asymptotic value, characterizing the very stable regime (Zilitinkevich et al. 2013; Bou-Zeid et al. 2018; Basu and Holtslag 2021, among other). Furthermore, under very stable stratification it is possible that wave phenomena increase the momentum diffusivity but not the heat diffusivity (Grachev et al. 2007). In such situation, generally $Pr_T > 1$. In a model that uses stability functions, the flux and gradient Richardson numbers are related as $Ri_f = f_h/f_m \; Ri_g$, where f_h is the stability function for heat. Therefore, the maximum flux Richardson number is limited by the imposed ratio f_h/f_m. As Pr_T is an important model tuning parameter (Sukoriansky et al. 2005) its values can affect the model performance.

In the presently proposed scheme, where a prognostic equation for heat flux is solved, the turbulent Prandtl number is not imposed and its value arises naturally from the solved ratio between Ri_f and Ri_g (Fig. 9). Fig. 9 shows that it is able to reproduce the relationship between Ri_f and Ri_g for both SBL regimes. In the weakly stable regime, Pr_T is approximately constant for $Ri_g < 0.2$, while the turbulent Prandtl number increases linearly with Ri_g if $Ri_g > 0.2$. A very similar pattern is presented by both observational

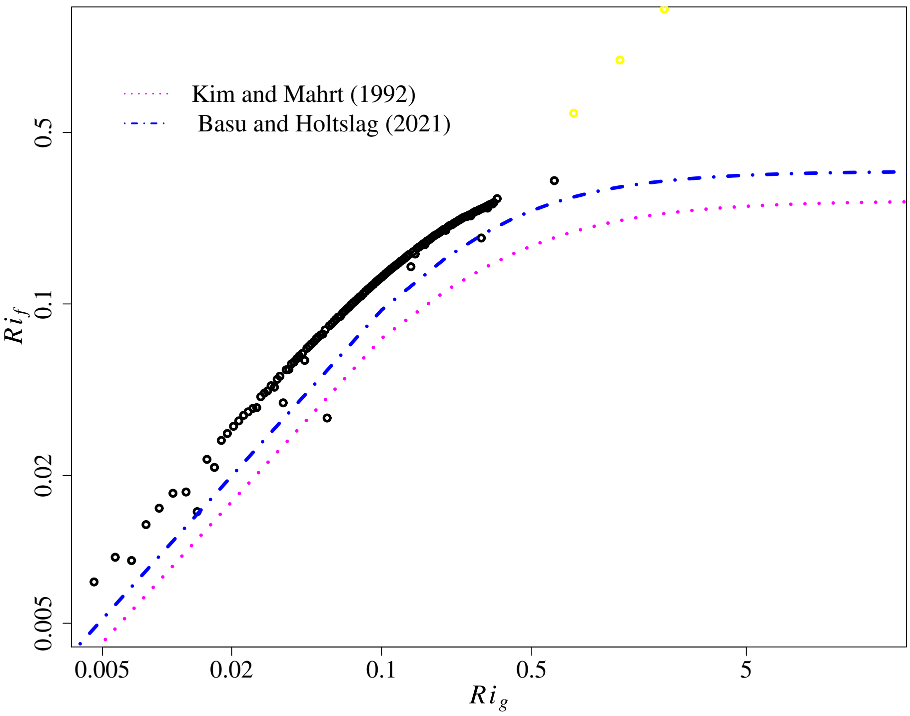

Fig. 9 Average flux Richardson number as a function of the gradient Richardson number, showing bin-averaged values taken from the all night of simulation, considering all runs

and model studies (Kim and Mahrt 1992; Zilitinkevich et al. 2013; Basu and Holtslag 2021) (Fig. 9). In very stable conditions, $Ri_g > 0.5$, the model results are limited by the imposed minimum TKE value assumed equal 0.00001 m^2 s^{-2} (yellow circles Fig 9).

5 Conclusion

A new boundary layer parameterization, in which the turbulent heat flux and the temperature variance are solved through a prognostic equation, has been introduced. The new scheme has been validated through simulations using the single-column Weather Research and Forecasting (WRF) model with the GABLS I experiment as a case-control.

A more realistic simulation of the nocturnal turbulence regimes of very stable and weakly stable boundary layers was the main motivation behind the idea of introducing a scheme that prognostically solves the heat flux and temperature variance. This goal has been achieved to a large degree, as shown by the comparison between mean and turbulent quantities presented in Section 4.

The present parameterization does not assume any prescribed stability function, differently from others SBL schemes. Here, the stratification dependence on other characteristics of the mean and turbulent flows arises naturally from the use of a prognostic equation for the heat flux . This way, the present scheme is able to realistically simulate the large temperature gradient that often occurs when mean wind speeds are very small. On the other hand, for large wind speeds, the temperature gradient is nearly destroyed, so that the model simulates a near-neutral SBL. Besides, the new formulation leads to smaller thermal gradients and a more abrupt transition between the SBL regimes than occurs in the Mellor-Yamada Nakanishi Niino 2.5 scheme, which was found by Maroneze et al. (2021) to best simulate the differences between the two regimes among the WRF schemes that solve TKE prognostically. This is also in better agreement with CASES-99 observations. Along the same line, SBL schemes typically use a fixed and prescribed turbulent Prandtl number, which may cause a excessive turbulent heat diffusion under very stable conditions (Grachev et al. 2007; Zilitinkevich et al. 2013; Maroneze et al. 2021). In the present parametrization, the turbulent Prandtl number is not prescribed, being directly calculated from the ratio between Ri_f and Ri_g.

The future steps of this research include the specific development and validation of a parametrization for the convective boundary layer, the inclusion of a more sophisticated parametrization for $\overline{w'^2}$ and the inclusion of humidity effects in the parameterization. Furthermore, three-dimensional model simulation of real cases, where advection and other external processes affect the PBL are necessary to validate the parameterization in a more realistic scenario, so that it can ultimately be implemented in operational models.

Acknowledgements OCA and FDC have financial support from CNPq (Conselho Nacional de Desenvolvimento Científico e Tecnológico).

References

Acevedo OC, Costa FD, Oliveira PE, Puhales FS, Degrazia GA, Roberti DR (2014) The influence of submeso processes on stable boundary layer similarity relationships. J Atmos Sci 71(1):207–225

Acevedo OC, Mahrt L, Puhales FS, Costa FD, Medeiros LE, Degrazia GA (2016) Contrasting structures between the decoupled and coupled states of the stable boundary layer. Q J R Meteorol Soc 142(695):693–702, DOI 10.1002/qj.2693

Acevedo OC, Maroneze R, Costa FD, Puhales FS, Degrazia GA, Nogueira Martins LG, Soares de Oliveira PE, Mortarini L (2019) The nocturnal boundary layer transition from weakly to very stable.Part I: Observations. Q J R Meteorol Soc 145(725):3577–3592, DOI 10.1002/qj.3642

Acevedo OC, Costa FD, Maroneze R, Carvalho AD, Puhales FS, Oliveira PE (2021) External controls on the transition between stable boundary-layer turbulence regimes. Quarterly Journal of the Royal Meteorological Society 147(737):2335–2351

André J, De Moor G, Lacarrere P, Du Vachat R (1978) Modeling the 24-hour evolution of the mean and turbulent structures of the planetary boundary layer. J Atmos Sci 35(10):1861–1883

Audouin O, Roehrig R, Couvreux F, Williamson D (2021) Modeling the gabls4 strongly-stable boundary layer with a gcm turbulence parameterization: Parametric sensitivity or intrinsic limits? Journal of Advances in Modeling Earth Systems 13(3):e2020MS002,269

Baas P, de Roode SR, Lenderink G (2008) The scaling behaviour of a turbulent kinetic energy closure model for stably stratified conditions. Boundary-layer meteorology 127(1):17–36

Baas P, van de Wiel BJ, van Meijgaard E, Vignon E, Genthon C, van der Linden SJ, de Roode SR (2019) Transitions in the wintertime near-surface temperature inversion at Dome C, Antarctica. Q J R Meteorol Soc 145(720):930–946

Basu S, Holtslag AA (2021) Turbulent prandtl number and characteristic length scales in stably stratified flows: steady-state analytical solutions. Environmental Fluid Mechanics 21(6):1273–1302

Battisti A, Acevedo OC, Costa FD, Puhales FS, Anabor V, Degrazia GA (2017) Evaluation of nocturnal temperature forecasts provided by the Weather Research and Forecast model for different stability regimes and terrain characteristics. Boundary-Layer Meteorol 162(3):523–546

Beare RJ, Macvean MK, Holtslag AA, Cuxart J, Esau I, Golaz JC, Jimenez MA, Khairoutdinov M, Kosovic B, Lewellen D, et al. (2006) An intercomparison of large-eddy simulations of the stable boundary layer. Boundary-Layer Meteorology 118(2):247–272

Blackadar A (1979) High resolution models of the planetary boundary layer. Adv Environ Sci Eng 1(1):50–85

Blackadar AK (1962) The vertical distribution of wind and turbulent exchange in a neutral atmosphere. J Geophys Res 67(8):3095–3102, DOI 10.1029/JZ067i008p03095

Bou-Zeid E, Gao X, Ansorge C, Katul GG (2018) On the role of return to isotropy in wall-bounded turbulent flows with buoyancy. J Fluid Mech 856:61–78

Bougeault P, Lacarrere P (1989) Parameterization of orography-induced turbulence in a mesobeta–scale model. Mon Wea Rev 117(8):1872–1890

Bretherton CS, Park S (2009) A new moist turbulence parameterization in the community atmosphere model. J Clim 22(12):3422–3448, DOI 10.1175/2008JCLI2556.1

Chen SH, Sun WY (2002) A one-dimensional time dependent cloud model. J Met Soc Japan 80(1):99–118, DOI 10.2151/jmsj.80.99

Cheng Y, Canuto V, Howard A, Ackerman A, Kelley M, Fridlind A, Schmidt G, Yao M, Del Genio A, Elsaesser G (2020) A second-order closure turbulence model: new heat flux equations and no critical richardson number. Journal of the Atmospheric Sciences 77(8):2743–2759

Costa FD, Acevedo OC, Medeiros LE, Maroneze R, Puhales FS, Carvalho Jr AD, Camponogara LF, dos Santos DM, Mortarini L (2020) Stable boundary layer regimes in single-column models. J Atmos Sci 77(6):2039–2054, DOI 10.1175/JAS-D-19-0218.1

Cuxart J, Holtslag AAM, Beare RJ, Bazile E, Beljaars A, Cheng A, Conangla L, Ek M, Freedman F, Hamdi R, Kerstein A, Kitagawa H, Lenderink G, Lewellen D, Mailhot J, Mauritsen T, Perov V, Schayes G, Steeneveld GJ, Svensson G, Taylor P, Weng W, Wunsch S, Xu KM (2006) Single-column model intercomparison for a stably stratified atmospheric boundary layer. Boundary-Layer Meteorol 118(2):273–303

Dudhia J (1989) Numerical study of convection observed during the winter monsoon experiment using a mesoscale two-dimensional model. J Atmos Sci 46(20):3077–3107

Duynkerke PG (1988) Application of the e$-\epsilon$ turbulence closure model to the neutral and stable atmospheric boundary layer. J Atmos Sci 45(5):865–880, DOI 10.1175/1520-0469(1988)045¡0865:AOTTCM¿2.0.CO;2

Grachev AA, Andreas EL, Fairall CW, Guest PS, Persson POG (2007) On the turbulent prandtl number in the stable atmospheric boundary layer. Boundary-layer meteorology 125(2):329–341

Holdsworth AM, Monahan AH (2019) Turbulent collapse and recovery in the stable boundary layer using an idealized model of pressure-driven flow with a surface energy budget. J Atmos Sci 76(5):1307–1327

van Hooijdonk IGS, Donda JMM, Clercx HJH, Bosveld FC, van de Wiel BJH (2015) Shear capacity as prognostic for nocturnal boundary layer regimes. J Atmos Sci 72(4):1518–1532, DOI 10.1175/JAS-D-14-0140.1

Janjić ZI (1994) The step-mountain Eta coordinate model: Further developments of the convection, viscous sublayer, and turbulence closure schemes. Mon Wea Rev 122(5):927–945

Kähnert M, Sodemann H, Remes TM, Fortelius C, Bazile E, Esau I (2022) Spatial variability of nocturnal stability regimes in an operational weather prediction model. Boundary-Layer Meteorology pp 1–25

Kim J, Mahrt L (1992) Simple formulation of turbulent mixing in the stable free atmosphere and nocturnal boundary layer. Tellus A 44(5):381–394

Klein PM, Hu XM, Shapiro A, Xue M (2016) Linkages between boundary-layer structure and the development of nocturnal low-level jets in Central Oklahoma. Boundary-Layer Meteorol 158(3):383–408

Kosović B, Curry JA (2000) A large eddy simulation study of a quasi-steady, stably stratified atmospheric boundary layer. Journal of the atmospheric sciences 57(8):1052–1068

Lapo K, Nijssen B, Lundquist JD (2019) Evaluation of turbulence stability schemes of land models for stable conditions. J Geophys Res 124(6):3072–3089, DOI 10.1029/2018JD028970

van der Linden SJA, Baas P, van Hooft JA, van Hooijdonk IGS, Bosveld FC, van de Wiel BJH (2017) Local characteristics of the nocturnal boundary layer in response to external pressure forcing. J Appl Meteorol Climat 56(11):3035–3047, DOI 10.1175/JAMC-D-17-0011.1

Lorenz T, Mayer S, Kral ST, Suomi I, Steeneveld GJ, Holtslag AA (2022) The stable atmospheric boundary layer over snow-covered sea ice: Model evaluation with fine-scale isobar18 observations. Quarterly Journal of the Royal Meteorological Society

Louis JF (1979) A parametric model of vertical eddy fluxes in the atmosphere. Boundary-Layer Meteorol 17(2):187–202, DOI 10.1007/BF00117978

Mahrt L (1998) Nocturnal boundary-layer regimes. Boundary-Layer Meteorol 88(2):255–278, DOI 10.1023/A:1001171313493

Mahrt L (2014) Stably stratified atmospheric boundary layers. Ann Rev Fluid Mech 46(1):23–45, DOI 10.1146/annurev-fluid-010313-141354

Maroneze R, Acevedo OC, Costa FD, Sun J (2019) Simulating the regime transition of the stable boundary layer using different simplified models. Boundary-Layer Meteorol 170(2):305–321, DOI 10.1007/s10546-018-0401-3

Maroneze R, Acevedo OC, Costa FD, Puhales FS, Anabor V, Lemes DN, Mortarini L (2021) How is the two-regime stable boundary layer reproduced by the different turbulence parametrizations in the weather research and forecasting model? Boundary-Layer Meteorology 178(3):383–413

Mellor GL, Yamada T (1974) A hierarchy of turbulence closure models for planetary boundary layers. J Atmos Sci 31(7):1791–1806

Mellor GL, Yamada T (1982) Development of a turbulence closure model for geophysical fluid problems. Rev Geophys 20(4):851–875

Mlawer EJ, Taubman SJ, Brown PD, Iacono MJ, Clough SA (1997) Radiative transfer for inhomogeneous atmospheres: RRTM, a validated correlated-k model for the longwave. J Geophys Res 102(D14):16,663–16,682, DOI 10.1029/97JD00237

Monahan AH, Rees T, He Y, McFarlane N (2015) Multiple regimes of wind, stratification, and turbulence in the stable boundary layer. J Atmos Sci 72(8):3178–3198, DOI 10.1175/JAS-D-14-0311.1

Mukul Tewari N, Tewari M, Chen F, Wang W, Dudhia J, LeMone M, Mitchell K, Ek M, Gayno G, Wegiel J, et al. (2004) Implementation and verification of the unified NOAH land surface model in the WRF model (formerly paper number 17.5). In: 20th Conference on Weather Analysis and Forecasting/16th Conference on Numerical Weather Prediction, pp 11–15

Nakanishi M, Niino H (2009) Development of an improved turbulence closure model for the atmospheric boundary layer. J Met Soc Japan 87(5):895–912, DOI 10.2151/jmsj.87.895

Powers JG, Klemp JB, Skamarock WC, Davis CA, Dudhia J, Gill DO, Coen JL, Gochis DJ, Ahmadov R, Peckham SE, Grell GA, Michalakes J, Trahan S, Benjamin SG, Alexander CR, Dimego GJ, Wang W, Schwartz CS, Romine GS, Liu Z, Snyder C, Chen F, Barlage MJ, Yu W, Duda MG (2017) The Weather Research and Forecasting model: Overview, system efforts, and future directions. Bull Amer Meteorol Soc 98(8):1717–1737

Skamarock WC, Klemp JB, Dudhia J, Gill DO, Barker DM, Wang W, Powers JG (2008) A description of the advanced research WRF version 3. NCAR technical note-475+ STR. https://opensky.ucar.edu/islandora/object/technotes:500

Stull RB (1988) An Introduction to Boundary Layer Meteorology. Kluwer Academic Publishers, Dordrecht, The Netherlands
Sukoriansky S, Galperin B, Perov V (2005) Application of a new spectral theory of stably stratified turbulence to the atmospheric boundary layer over sea ice. Boundary-Layer Meteorol 117(2):231–257, DOI 10.1007/s10546-004-6848-4
Sun J, Mahrt L, Banta RM, Pichugina YL (2012) Turbulence regimes and turbulence intermittency in the stable boundary layer during "CASES-99". J Atmos Sci 69(1):338–351
Sun J, Lenschow DH, LeMone MA, Mahrt L (2016) The role of large-coherent-eddy transport in the atmospheric surface layer based on "cases-99" observations. Boundary-Layer Meteorol 160(1):83–111, DOI 10.1007/s10546-016-0134-0
Taylor MG (1915) I. eddy motion in the atmosphere. Phil Trans R Soc Lond A 215(523-537):1–26
Taylor PA, Delage Y (1971) A note on finite-difference schemes for the surface and planetary boundary layers. Boundary-Layer Meteorology 2(1):108–121
Therry G, Lacarrere P (1983) Improving the eddy kinetic energy model for planetary boundary layer description. Boundary-Layer Meteorol 25(1):63–88, DOI 10.1007/BF00122098
Vignon E, van de Wiel BJ, van Hooijdonk IG, Genthon C, van der Linden SJ, van Hooft JA, Baas P, Maurel W, Traullé O, Casasanta G (2017) Stable boundary-layer regimes at transitions in the wintertime near-surface temperature inversion at Dome C, Antarctica: observation and analysis. Q J R Meteorol Soc 143(704):1241–1253
Weng W, Taylor PA (2003) On modelling the one-dimensional atmospheric boundary layer. Boundary-layer meteorology 107(2):371–400
van de Wiel BJH, Moene AF, Jonker HJJ, Baas P, Basu S, Donda JMM, Sun J, Holtslag AAM (2012) The minimum wind speed for sustainable turbulence in the nocturnal boundary layer. J Atmos Sci 69(11):3116–3127, DOI 10.1175/JAS-D-12-0107.1
van de Wiel BJH, Vignon E, Baas P, van Hooijdonk IGS, van der Linden SJA, Antoon van Hooft J, Bosveld FC, de Roode SR, Moene AF, Genthon C (2017) Regime transitions in near-surface temperature inversions: A conceptual model. J Atmos Sci 74(4):1057–1073, DOI 10.1175/JAS-D-16-0180.1
Wyngaard JC (1975) Modeling the planetary boundary layer — extension to the stable case. Boundary-Layer Meteorol 9(4):441–460, DOI 10.1007/BF00223393
Zilitinkevich SS, Elperin T, Kleeorin N, Rogachevskii I, Esau I (2013) A hierarchy of energy- and flux-budget (EFB) turbulence closure models for stably-stratified geophysical flows. Boundary-Layer Meteorol 146(3):341–373